Abundance of Weyl points in semiclassical multiterminal superconducting nanostructures

Hristo Barakov and Yuli V. Nazarov ⓘ

Kavli Institute of Nanoscience, Delft University of Technology, 2628 CJ Delft, The Netherlands

We show that the quasicontinuous gapless spectrum of Andreev bound states in multiterminal semi-classical superconducting nanostructures exhibits a large number of topological singularities. We concentrate on Weyl points in a four-terminal nanostructure and compute their density and correlations in three-dimensional parameter space for a universal random matrix theory model as well as for the concrete nanostructures described by the quantum circuit theory. We mention the opportunities for experimental observation of the effect in a quasicontinuous spectrum.

The topological properties of quantum spectra in condensed matter systems received considerable attention in the past decade and are still under active consideration [1–4]. A large research field that has been formed thereby addresses gapped phases of insulators [5] and superconductors [6] characterized by globally defined topological numbers and the edge modes [7] at the interfaces separating such phases. In addition to this, the spectra can exhibit topological singularities in the form of level crossings where the topological charge is defined at the singularity rather than globally. The simplest example of such singularity is a Weyl point (WP) [8] corresponding to the crossing of two levels in a point in three-dimensional (3D) space of parameters. Physical realizations of WPs include special points in the bandstructure of 3D solids [9], spectra of polyatomic molecules [10] and nanomagnets [11], and quantum transport systems [12].

The occurrence of WPs were recently predicted in the spectrum of Andreev bound states (ABS) of generic four-terminal superconducting nanostructures [13] where the 3D parameter space is formed by three independent superconducting phases of the terminals. Most important, WPs are the crossings at *zero energy* that define the topology of the ground state. These WPs in 3D give rise to two-dimensional (2D) global Chern numbers that are directly manifested as quantized transconductances of the nanostructure. The ideal periodicity of the space of superconducting phases allows to model higher-dimensional band structures with the multiterminal superconducting nanostructures (MTSN). These ideas resulted in an outburst of theoretical [14–20] and experimental [21–25] activities in the field of MTSN.

In this paper, we address semiclassical MTSN: those with a size much exceeding the electron wave length, a large number of transport channels $G/G_Q \gg 1$ (with G being a typical conductance of the nanostructure and $G_Q \equiv e^2/\pi\hbar$ being the conductance quantum), and a large number of ABS. The Hamiltonian description of semiclassical structures is hardly practical in view of the large number of parameters: instead, their properties are mainly determined by a handful of design

parameters. Those include the distribution of diffusive resistivity over the structure, the presence of tunnel junctions and ballistic contacts, and can be encountered for in the framework of the finite-element quantum circuit theory [26]. The rest of the Hamiltonian parameters are considered as random ones in line with the general approach of mesoscopic fluctuations and quantum chaos [27–33]. The average properties of the resulting quasicontinuous spectrum-like energy-dependent density of states are determined by design parameters, the correlations of the level positions in the spectrum are obtained by the methods of random matrix theory (RMT) taking design parameters into account.

Recent developments concern the understanding of the quasicontinuous spectrum in MTNS. It was predicted [34] that this spectrum can be either gapped or gapless depending on the design parameters of the MTSN and the point in the space of the superconducting phases. A specific topology can be introduced in semiclassical MTSN. It was discovered and confirmed experimentally [35,36] that the gapped phases are characterized by topological numbers and the gapless phase is explained by topological protection of these numbers [37]. The protection-unprotection transition has been discussed in this context [38].

In this paper, we reveal the abundance of zero-energy topological singularities [Fig. 1(c)] in the parameter region of the gapless quasicontinuous spectrum. In four-terminal structures, those are isolated WPs separated by a typical distance $l_c \simeq (G/G_Q)^{-1/2} \ll 2\pi$. The positions of WPs are randomly determined by details of the electron interference in the structure, while their averaged density and its correlations are determined by the structure design. We relate the density of WPs to the parameter l_c governing the universal parametric correlations [28,29] in random matrix ensembles, show how to compute this density for concrete nanostructures, investigate the density correlations manifested as the transconductace of the structure, and shortly discuss the opportunities of the experimental detection of the WPs in semiclassical MTSN's. We concentrate on a realistic situation of negligible spin-orbit interaction [37]. The research presented substantially
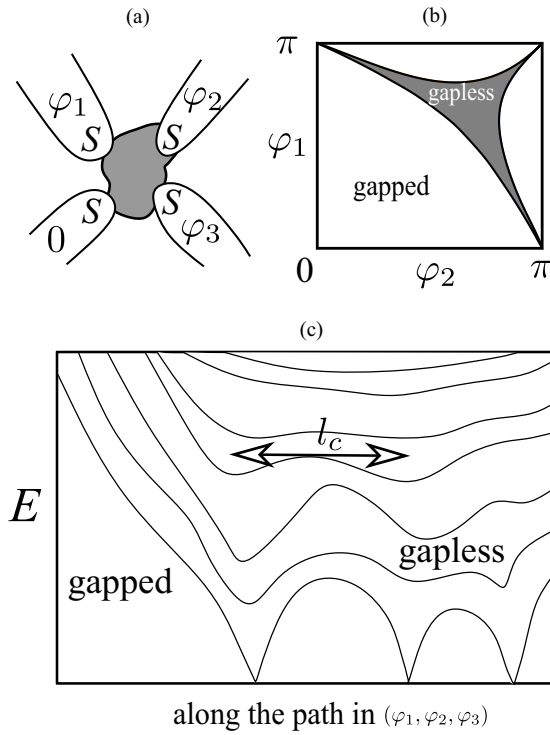
FIG. 1. Weyl points in semi-classical MTSN. (a) Four-terminal semiconducting nanostructure, three independent phases forming a parameter space. (b) The domains of gapped and gapless phases at $\varphi_3 = 0$. (c) The discrete spectrum near the boundary of gapped and gapless domains plotted along a path in 3D parametric space that goes via the WPs. The distance between the WP's is of the order of the local value of l_c, a parameter governing the universal parametric correlations in the corresponding random matrix ensemble.

extends the mesoscopic fluctuation approach formulated in [27–33,39–41].

Let us start with qualitative estimations. Given a four-terminal nanostructure of a typical conductance G one expects $\simeq G/G_Q$, $G_Q \equiv e^2/\pi\hbar$, conduction channels, and, correspondingly, $\simeq G/G_Q$ discrete ABS affected by superconductivity. This estimation is valid both for "short" nanostructures with the typical size being smaller than the superconducting coherence length, where these levels are spread in the energy interval Δ, with Δ being the superconducting energy gap and "large" nanostructure where these levels are concentrated in a much smaller energy interval $E_{\text{Th}} \simeq (G/G_Q)\delta_S$, δ_S being the mean level spacing in the normal state. The energies of these levels depend on the three superconducting phases. Owing to periodicity in phases, the spectrum is to be considered in a Brillouin zone (BZ) of the size $\simeq 2\pi$. The RMT of parametric correlations suggests that the level energies wiggle randomly. The energies change at the scale of the level spacing at a typical distance l_c in the parameter space [28,29]. This distance is determined from a comparison of the mean fluctuations of the derivatives of the energies with respect to the parameters and this level spacing. For our situation, the estimation $l_c \simeq \sqrt{G_Q/G}$ in the space of phases holds for both long and short nanostructures. To understand WP's we concentrate on the level that is closest to zero energy. Upon wiggling, it will reach zero at a typical distance of the order
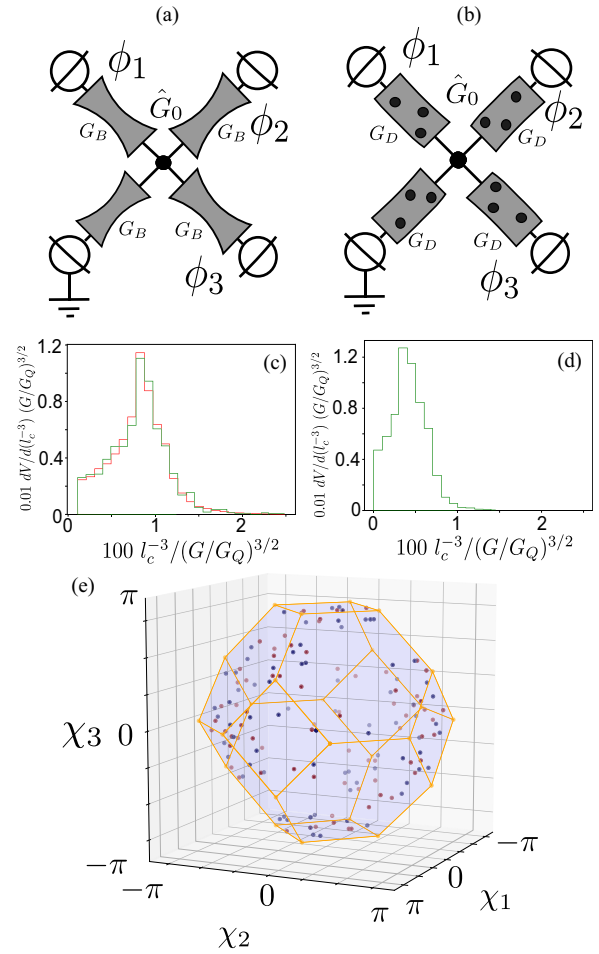

FIG. 2. Weyl points in concrete nanostructures. Example circuits: (a) ballistic and (b) diffusive crosses of identical arm conductances G. The numerical histograms for $dV/d(l_c^{-3})$ for the (c) ballistic (c) and (d) diffusive cross. In (c), we compare estimations obtained from the analytical formula (green lines) and the actual positions of the WPs found (red lines) to demonstrate the correspondence within the statistical error. An example of (e) WP positions found $G/G_Q = 50$.

of l_c. Therefore, the total number of WP's in the Brillouin zone can be estimated as $N_w \simeq (l_c)^{-3} \simeq (G/G_Q)^{3/2}$. Similar estimations hold for any number of terminals N_t. The Weyl singularities are, in this case, manifolds of dimension $N_t - 4$ (e.g., lines for $N_t = 5$) and l_c estimates a typical distance between the singularities as well as their typical wiggling scale.

Our detailed results (see Fig. 2) give

$$N_w = A(G/G_Q)^{3/2} \tag{1}$$

for the cross-like structures with the arm conductances G where $A = 0.40$ for the ballistic conductor and $A = 0.16$ for the diffusive one. The dimensionless coefficient $A < 1$, this is explained by a rather small fraction of the BZ volume taken by the gapless phase (25% for ballistic and 18% for diffusive cross) and a relatively large numerical coefficient B for the relevant $l_c = B(G/G_Q)^{-1/2}$ [$B \approx 5(6)$ for the ballistic(diffusive)

cross is determined from the maximum of the distributions plotted in Figs. 2(c) and 2(d)].

As it was shown in [13] the transconductance of the structure is defined by a Chern number C of a plane traversing the BZ. The difference of the two Chern numbers corresponding to two different planes is given by the total charge of the WP's enclosed between the planes. If the WP positions were uncorrelated, the estimation of the variance of this difference would be just the number of WP's enclosed, with $\langle\langle(C_1 - C_2)^2\rangle\rangle \simeq N_w \simeq dl_c^{-3}$, $2\pi \gg d \gg l_c$ being the separation of the planes. This estimation is incorrect: the WPs do correlate similar to ions in an electroneutral gas, so a charge of a WP is screened by other points at the distance of the order of their separation, that is, of l_c. Therefore, only WP's at a distance $\simeq l_c$ contribute to the fluctuation of the Chern number and $\langle\langle(C_1 - C_2)^2\rangle\rangle \simeq l_c^{-2} \simeq (G/G_Q)$. A typical transconductance is thus $\simeq \sqrt{G_Q G}$.

Our quantitative results are obtained in the course of three activities. (i) We study numerically a generic RM model to relate the density of WPs to l_c^{-3} and quantify the correlations of WP's. (ii) We develop a theory to compute $l_c^{-3}(\boldsymbol{\phi})$ for any MTSN described by the quantum circuit theory [26] and derive concrete expressions for a single-node circuit. (iii) We find numerically the positions of WP's in the ballistic cross junction [Fig. 2(a)] to prove the consistency of the results obtained in the activities (i) and (ii). The details of all activities are given in [42].

Activity A. The studies of statistics of spectral crossings were pioneered by Wilkinson *et al.* [39–41]. They introduced a convenient RMT model in a 3D parameter space $\{\phi_i\}$,

$$H(\boldsymbol{\phi}) = \sum_{i=1}^{3} (\sin \phi_i X_i + \cos \phi_i Y_i). \tag{2}$$

In this model, X_i, Y_i are $2N \times 2N$ random Hermitian matrices with independent normally distributed elements of variance $1/3$, $N \gg 1$. Since we address the WPs in superconducting stuctures at zero energy, in distinction from [39–41], we choose these random matrices to obey Bogoliubov—de Gennes (BdG) mirror symmetry of the spectrum (class C [30]). Generally, l_c is defined as $l_c^{-3} = \sqrt{\det\langle\langle v_i v_j\rangle\rangle}/\delta_S^3$, $v_i \equiv \partial E/\partial\phi_i$, δ_S is the mean level spacing at the corresponding energy. For the model in use, $l_c = \pi\sqrt{3/2N}$ conveniently does not depend on $\boldsymbol{\phi}$ so that the WP density is uniform. We search the positions of WPs by an iterative minimization of the energy of the closest to zero level. To make sure we find all the WPs, we repeat the iteration cycle starting it from a randomly chosen point in the parameter space. We have to do this a number of times that by a factor exceeds the expected number of points. The execution time of the algorithm thus scales as $N^{9/2}$ so we cannot access very large N and work with $N = 40$–80. For the WP concentration, we compute

$$N_w/V = (0.83 \pm 0.05)l_c^{-3}. \tag{3}$$

This is lower than the concentration of the level crossings in the Gaussian unitary ensemble (GUE) [40] $(2/3)\sqrt{\pi}l_c^{-3} \approx 1.18l_c^{-3}$. We reproduce this result searching for the crossings of the tenth and eleventh levels. The charge density for a WP
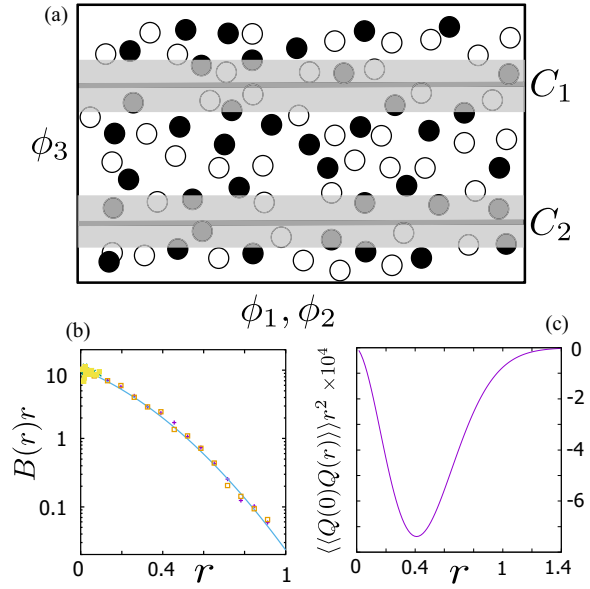

FIG. 3. Correlations of Weyl points. (a) The distribution of WP charge is "electroneutral." Owing to this, the fluctuations of Chern numbers in the planes 1, 2 are contributed to by WPs at the distance $\simeq l_c$ from the planes (in grey strips). (b) The numerical results for the correlator of Berry curvatures and the fit. The crosses, empty, and filled squares are the results of independent runs, their scattering characterizes the accuracy of the results. (c) The charge-charge correlator as computed from the fit.

realization is defined by

$$Q(\mathbf{r}) = \sum_i q_i \delta(\mathbf{r} - \mathbf{r}_i), \tag{4}$$

with $q_i = \pm 1$, r_i being the charges and positions of the WPs. We address the correlator of the charge density $\langle\langle Q(0)Q(\mathbf{r})\rangle\rangle$, with $\mathbf{r}$ being the vector distance in units of l_c. To enhance the statistics, we evaluated an equivalent correlator of Berry curvatures of the closest-to-zero level. The results of 10^5 runs per point are presented in Fig. 3 and can be fitted with

$$\langle B^\alpha(0)B^\beta(\mathbf{r})\rangle = \delta_{\alpha\beta}B(r), \quad rB(r) \approx 10.4e^{-2.8r-3.3r^2}. \tag{5}$$

Since the charge density of WPs is given by the divergence of Berry curvature ([43,44])

$$\langle\langle Q(0)Q(\mathbf{r})\rangle\rangle = (4\pi)^{-2}\nabla^2 B(r), \tag{6}$$

see Fig. 3(c) for the plot. By virtue of the electroneutrality of WP gas $\int d\mathbf{r}\langle\langle Q(0)Q(\mathbf{r})\rangle\rangle = -N_w/V$. The fluctuations of the Chern number over a surface of the size $\gg l_c$ are governed by $D \equiv -\int d\mathbf{r}\, r\langle\langle Q(0)Q(\mathbf{r})\rangle\rangle$,

$$\langle\langle C^2\rangle\rangle = D \int dS\, l_c^{-2}(\boldsymbol{\phi}), \tag{7}$$

with dS being an area element of the surface $D \approx 0.5$ from our calculations.

Activity B. While there are no perturbative methods to compute the density of WPs directly, they are available for the mesoscopic parametric correlations [31,32]. With those, one can compute l_c^{-3} for any system characterized by electronic Green's functions. We make use of the quantum circuit theory

[26] that is a powerful finite-element technique for electronic Green's functions. In quantum circuit theory, the structure is subdivided into reservoirs and nodes, the network is formed by connectors of various kinds, for instance, ballistic, tunnel, or diffusive. The Green's functions are presented by the matrices $\hat{G}_a$, $\hat{G}^2 = 1$, $\mathrm{Tr}\hat{G} = 0$ defined in the nodes and the reservoirs. The semi-classical solution is obtained by minimization of an action with respect to $\hat{G}$ in the reservoirs at fixed $\hat{G}$ in the nodes.

The mesoscopic parametric correlations for a general circuit theory were derived in [33]. For this, one substitutes to the action $\hat{G}$ of double dimension, two diagonal blocks corresponding to the parameter sets 1, 2. Near the minimum, the action can be expanded up to quadratic terms with respect to nondiagonal deviations of $\check{G}$, $\check{M}$ being the matrix characterizing the quadratic expansion. The correlator of mesoscopic fluctuations of the action values at two parameter sets reads [33]

$$\langle\langle \mathcal{S}_1 \mathcal{S}_2 \rangle\rangle = \ln \det' \check{M}, \tag{8}$$

where "prime" excludes the zero eigenvalues of $\check{M}$ from the determinant.

We implement this general technique to compute l_c^{-3} for concrete superconducting nanostructures. It is known [27] that the energies of Andreev bound states are expressed in terms of the effective scattering matrix SS^*, with S being the electron scattering matrix in the space of all channels coming to the nanostructure, S^* being the hole scattering matrix, the superconducting phases included. The circuit-theory action at the imaginary energy $\Delta \sin \theta$ (see, e.g., [45]) before the averaging over the mesoscopic fluctuations can be expressed in terms of eigenvalues $SS^* \to -e^{i\lambda}$ of the effective scattering matrix, these eigenvalues coming in $\pm$ pairs

$$-\mathcal{S}(\theta, \boldsymbol{\phi}) = \sum_\lambda \ln\left(1 - \cos^2 \theta \cos^2 \frac{\lambda}{2}\right) \approx \sum_\lambda \ln(\theta + i\lambda), \tag{9}$$

the last equality holding for close-to-zero energies/eigenvalues. The correlator of the velocities in this limit is related to the correlator of the action values

$$\langle\langle \partial_\alpha \mathcal{S}(\theta) \partial_\beta \mathcal{S}(\theta') \rangle\rangle = \pi \frac{\langle\langle v_\alpha v_\beta \rangle\rangle \rho_\lambda}{|\theta| + |\theta'|}. \tag{10}$$

The action can be represented in a quantum circuit theory of 2×2 matrices and the correlator is to be computed with the aid of Eq. (8). In the Supplemental Material [42], we derive an explicit expression of l_c^{-3} for a single-node structure.

We concentrate on two simplest example MTSN [Figs. 2(a) and 2(b)]: a chaotic cavity connected to four leads by ballistic conductors of the same conductance G, ballistic cross, and the corresponding diffusive structure, diffusive cross. With the expressions obtained, we compute the distribution of l_c^{-3}, and consequently, the WP density, over the phase space, by evaluating l_c^{-3} in random points and collecting the data into histograms: this gives a fraction of the phase-space volume $dV/d(l_c^{-3})$ at a given l_c^{-3}. The histograms for these two examples are qualitatively similar but distinct. Summing up the histograms and employing the result (1) gives the already mentioned estimations of the number of WP's, Eq. (3).

Activity C. We explicitly compute the WP positions for random chaotic cavities. For this, we pick up the electron scattering matrix S from the circular orthogonal ensemble and find all phase settings at which SS^* has an eigenvalue -1 [27]. We find 75–95 WPs for $N = G/G_Q = 50$ conform to the results of the activities A and B and verify the scaling of the number of points with N. We also perform a more thorough check evaluating l_c^{-3} in the random positions found and collecting the data to the histogram. The resulting estimation of $dV/d(l_c^{-3})$ that involves 2686 WP's coincides with the results of activity B within the statistical error [Fig. 2(c)]. In Fig. 2(e), we plot the positions of WP's found for a realization of S at $G/G_Q = 50$. We choose the coordinate system in the space of phases to be consistent with the symmetry of the structure

$$\chi_1 = \tfrac{1}{2}(\phi_1 - \phi_2 - \phi_3), \tag{11}$$

where $\chi_{2,3}$ are defined by the above relation with cyclically permuted indexes. In these coordinates, the BZ is the truncated octahedron, as for a fcc lattice. The gapped region is in the center of the BZ, the gapless region encloses its boundary [46]. The special points where the gapless region becomes infinitesimally thin [38] are located in the centers of the squares and hexagons, and, as seen in the figure, the WPs are mostly concentrated in the corners of the BZ.

Let us shortly discuss the methods of experimental detection of WPs in MTSN. For sufficiently large level splitting $G \simeq G_Q$, the WPs can be found spectroscopically as the zeros of the lowest ABS. For $G \gg G_Q$ where the level splitting is small not exceeding $k_B T$, the detection is more challenging. We envisage three methods. (i) *Noise measurement of a response.* We note that each of the two states forming a WP cone gives a response, both inductive and Berry curvature, that diverges near the point. The divergencies are of opposite signs so thermal averaging cancels those in the average-in-time signal. However, the divergences are observable either as a telegraph signature in the time trace of a signal or in the divergent noise amplitude at frequencies of the order of the inverse switching time between the states. (ii) *Transconductance (noise) measurements*. We predict a transconductance $\simeq \sqrt{GG_Q}$. While in the presence of thermal averaging this transconductance is not quantized, its value, and the noise of this value, will exhibit fluctuations as a function of the control phase [13] that can be used for scanning the WP positions. (iii) *Transport spectroscopy*. If the MTSN is in a weak tunnel contact with a normal lead, the differential conductance of this tunnel junction exhibits anomalies at the WP positions, both at a low and high voltage bias [47].

In conclusion, we showed how to quantify the density and correlations of Weyl singularities in a quasicontinuous spectrum of a semiclassical MTNS of a given design combining RMT and quantum circuit theory. The source code and the raw data can be found at [48]. The field is open for experimental investigations.

[1] R.-X. Zhang and S. Das Sarma, Anomalous Floquet Chiral Topological Superconductivity in a Topological Insulator Sandwich Structure, Phys. Rev. Lett. **127**, 067001 (2021).

[2] Y. X. Zhao, C. Chen, X.-L. Sheng, and S. A. Yang, Switching Spinless and Spinful Topological Phases with Projective *pt* Symmetry, Phys. Rev. Lett. **126**, 196402 (2021).

[3] Z. Yang, Q. Yang, J. Hu, and D. E. Liu, Dissipative Floquet Majorana Modes in Proximity-Induced Topological Superconductors, Phys. Rev. Lett. **126**, 086801 (2021).

[4] R.-X. Zhang and S. Das Sarma, Intrinsic Time-Reversal-Invariant Topological Superconductivity in Thin Films of Iron-Based Superconductors, Phys. Rev. Lett. **126**, 137001 (2021).

[5] M. Z. Hasan and C. L. Kane, Colloquium: Topological insulators, Rev. Mod. Phys. **82**, 3045 (2010).

[6] X.-L. Qi and S.-C. Zhang, Topological insulators and superconductors, Rev. Mod. Phys. **83**, 1057 (2011).

[7] B. Bernevig and T. Hughes, *Topological Insulators and Topological Superconductors* (Princeton University Press, Princeton, NJ, 2013).

[8] H. Weyl, Electron und gravitation. I, Z. Phys. **56**, 330 (1929).

[9] N. P. Armitage, E. J. Mele, and A. Vishwanath, Weyl and dirac semimetals in three-dimensional solids, Rev. Mod. Phys. **90**, 015001 (2018).

[10] F. Faure and B. I. Zhilinskii, Topological Chern Indices in Molecular Spectra, Phys. Rev. Lett. **85**, 960 (2000).

[11] W. Wernsdorfer, N. E. Chakov, and G. G. Christou, Quantum Phase Interference and Parity Effects in Mn_{12} Single-Molecule Magnets, Phys. Rev. Lett. **95**, 037203 (2005).

[12] R. Leone, L. P. Lévy, and P. Lafarge, Cooper-Pair Pump as a Quantized Current Source, Phys. Rev. Lett. **100**, 117001 (2008).

[13] R.-P. Riwar, M. Houzet, J. S. Meyer, and Y. V. Nazarov, Multi-terminal Josephson junctions as topological matter, Nat. Commun. **7**, 11167 (2016).

[14] H.-Y. Xie and A. Levchenko, Topological supercurrents interaction and fluctuations in the multiterminal Josephson effect, Phys. Rev. B **99**, 094519 (2019).

[15] H.-Y. Xie, M. G. Vavilov, and A. Levchenko, Topological andreev bands in three-terminal Josephson junctions, Phys. Rev. B **96**, 161406(R) (2017).

[16] M. Houzet and J. S. Meyer, Majorana-Weyl crossings in topological multiterminal junctions, Phys. Rev. B **100**, 014521 (2019).

[17] R. L. Klees, G. Rastelli, J. C. Cuevas, and W. Belzig, Microwave Spectroscopy Reveals the Quantum Geometric Tensor of Topological Josephson Matter, Phys. Rev. Lett. **124**, 197002 (2020).

[18] V. Fatemi, A. R. Akhmerov, and L. Bretheau, Weyl Josephson circuits, Phys. Rev. Res. **3**, 013288 (2021).

[19] H. Weisbrich, G. Rastelli, and W. Belzig, Geometrical Rabi oscillations and Landau-Zener transitions in non-Abelian systems, Phys. Rev. Res. **3**, 033122 (2021).

[20] T. Yokoyama and Y. V. Nazarov, Singularities in the andreev spectrum of a multiterminal Josephson junction, Phys. Rev. B **92**, 155437 (2015).

[21] N. Pankratova, H. Lee, R. Kuzmin, K. Wickramasinghe, W. Mayer, J. Yuan, M. G. Vavilov, J. Shabani, and V. E. Manucharyan, Multiterminal Josephson Effect, Phys. Rev. X **10**, 031051 (2020).

[22] G. V. Graziano, J. S. Lee, M. Pendharkar, C. Palmstrom, and V. S. Pribiag, Transport studies in a gate-tunable three-terminal Josephson junction, Phys. Rev. B **101**, 054510 (2020).

[23] A. W. Draelos, M.-T. Wei, A. Seredinski, H. Li, Y. Mehta, K. Watanabe, T. Taniguchi, I. V. Borzenets, F. Amet, and G. Finkelstein, Supercurrent flow in multiterminal graphene Josephson junctions, Nano Lett. **19**, 1039 (2019).

[24] A. H. Pfeffer, J. E. Duvauchelle, H. Courtois, R. Mélin, D. Feinberg, and F. Lefloch, Subgap structure in the conductance of a three-terminal Josephson junction, Phys. Rev. B **90**, 075401 (2014).

[25] E. M. T. Fadaly, H. Zhang, S. Conesa-Boj, D. Car, Ö. Gül, S. R. Plissard, R. L. M. Op het Veld, S. Kölling, L. P. Kouwenhoven, and E. P. A. M. Bakkers, Observation of conductance quantization in InSb nanowire networks, Nano Lett. **17**, 6511 (2017).

[26] Y. V. Nazarov and Y. M. Blanter, *Quantum Transport: Introduction to Nanoscience* (Cambridge University Press, Cambridge, England, 2009).

[27] C. W. J. Beenakker, Random-matrix theory of quantum transport, Rev. Mod. Phys. **69**, 731 (1997).

[28] B. D. Simons and B. L. Altshuler, Universal Velocity Correlations in Disordered and Chaotic Systems, Phys. Rev. Lett. **70**, 4063 (1993).

[29] C. W. J. Beenakker, Brownian-Motion Model for Parametric Correlations in the Spectra of Disordered Metals, Phys. Rev. Lett. **70**, 4126 (1993).

[30] A. Altland and M. R. Zirnbauer, Nonstandard symmetry classes in mesoscopic normal-superconducting hybrid structures, Phys. Rev. B **55**, 1142 (1997).

[31] B. Spivak and A. Zyuzin, Mesoscopic fluctuations of current density in disordered conductors, in *Mesoscopic Phenomena in Solids*, Modern Problems in Condensed Matter Sciences, Vol. 30, edited by B. Althshuler, P. Lee, and R. Webb (Elsevier, New York, 1991), Chap. 2, pp. 37–80.

[32] S. Feng, Conductance Fluctuations and 1/f Noise Magnitudes in Small Disordered Structures: Theory, in *Conductance fluctuations and 1/f noise magnitudes in small disordered structures: Theory*, Modern Problems in Condensed Matter Sciences, Vol. 30, edited by B. Altshuler, P. Lee, and R. Webb (Elsevier, New York, 1991), Chap. 4, pp. 107–129.

[33] G. Campagnano and Y. V. Nazarov, G_Q corrections in the circuit theory of quantum transport, Phys. Rev. B **74**, 125307 (2006).

[34] C. Padurariu, T. Jonckheere, J. Rech, R. Mélin, D. Feinberg, T. Martin, and Y. V. Nazarov, Closing the proximity gap in a metallic Josephson junction between three superconductors, Phys. Rev. B **92**, 205409 (2015).

[35] E. Strambini, S. D'Ambrosio, F. Vischi, F. S. Bergeret, Y. V. Nazarov, and F. Giazotto, The ω-SQUIPT as a tool to phase-engineer Josephson topological materials, Nat. Nanotechnol. **11**, 1055 (2016).

[36] F. Vischi, M. Carrega, E. Strambini, S. D'Ambrosio, F. S. Bergeret, Y. V. Nazarov, and F. Giazotto, Coherent transport properties of a three-terminal hybrid superconducting interferometer, Phys. Rev. B **95**, 054504 (2017).

[37] T. Yokoyama, J. Reutlinger, W. Belzig, and Y. V. Nazarov, Order, disorder, and tunable gaps in the spectrum of Andreev bound states in a multiterminal superconducting device, Phys. Rev. B **95**, 045411 (2017).

[38] X.-L. Huang and Y. V. Nazarov, Topology protection–unprotection transition: Example from multiterminal superconducting nanostructures, Phys. Rev. B **100**, 085408 (2019).

[39] M. Wilkinson and E. J. Austin, Densities of degeneracies and near-degeneracies, Phys. Rev. A **47**, 2601 (1993).

[40] P. N. Walker and M. Wilkinson, Universal Fluctuations of Chern Integers, Phys. Rev. Lett. **74**, 4055 (1995).

[41] P. N. Walker, M. J. Sánchez, and M. Wilkinson, Singularities in the spectra of random matrices, J. Math. Phys. **37**, 5019 (1996).

[42] See Supplemental Material at http://link.aps.org/supplemental/10.1103/PhysRevB.107.014507 for a detailed explanation of all activities of this project.

[43] M. V. Berry and P. Shukla, Geometric phase curvature statistics, J. Stat. Phys. **180**, 297 (2020).

[44] O. Gat and M. Wilkinson, Correlations of quantum curvature and variance of Chern numbers, SciPost Phys. **10**, 149 (2021).

[45] E. V. Repin, Y. Chen, and Y. V. Nazarov, Topological properties of multiterminal superconducting nanostructures: Effect of a continuous spectrum, Phys. Rev. B **99**, 165414 (2019).

[46] B. van Heck, S. Mi, and A. R. Akhmerov, Single fermion manipulation via superconducting phase differences in multiterminal Josephson junctions, Phys. Rev. B **90**, 155450 (2014).

[47] Y. Chen and Y. V. Nazarov, Spintronics with a weyl point in superconducting nanostructures, Phys. Rev. B **103**, 165424 (2021).

[48] H. Barakov and Y. Nazarov, Abundance of Weyl points in semiclassical multiterminal superconducting nanostructures [Data set], Zenodo 10.5281/zenodo.5806468 (2021).